

# S-wave Splitting Analysis: Covariance Matrix Method and Preliminary Application

Xu Li, Edmund Sze, Dan Burns and M. Nafi Toksoz  
Earth Resources Laboratory  
Dept. of Earth, Atmospheric and Planetary Sciences  
Massachusetts Institute of Technology  
Cambridge, MA 02142

## Abstract

From polarization analysis on a covariance matrix, a method of S-wave splitting analysis is developed, which processes 3-component recordings simultaneously, rather than just 2 horizontal components as done traditionally. Thus not only orientation, but also dip information of fractures can be resolved. The synthetic test results show that this method is stable even for noise levels as high as 100% (S/N=1). If time window sizes are larger than roughly twice the time delay between the fast and slow S waves, the results are always reasonable even with noise levels up to 50%. The method is applied to 12 microseismic events recorded from a producing reservoir. The preliminary results suggest that stress-aligned fractures strike in NE-SW direction in the reservoir. The dips of the fractures are primarily vertical. The time difference between the fast and slow shear waves is about several tens of milliseconds per kilometer.

## 1. Introduction

S-wave splitting is a pervasive phenomenon related with seismic velocity anisotropy. When a seismic wave propagates through anisotropic media, the S-wave always splits into two approximately orthogonal polarized phases with different velocities, so called fast and slow waves respectively. This phenomenon is widely observed for rays propagating through either crust or mantle. For rays traveling through the earth mantle, people use SKS, SKKS, PKS splitting to extract the anisotropy characteristics of the mantle (*i. e.*, Menke & Levin, 2003, Gok *et al.*, 2003). For the rays sampling the upper half crust, people analyze the shear wave splitting to extract the orientation of stress-aligned cracks (Kaneshima, 1990, Crampin & Lovell, 1991, Crampin *et al.*, 2002), and use temporal variations of the time delay between the fast and slow S-waves to predicate the occurrence of a large event (*i. e.*, Gao *et al.*, 1998, Crampin *et al.* 1999).

For shear-wave splitting in the crustal rocks, the primary anisotropy mechanism appears to be the distribution of stress-aligned cracks, microcracks, and preferentially oriented pore space known as extensive-dilatancy anisotropy (EDA) (Crampin, Evans & Atkinson 1984, Crampin, 1993) rather than the rock foliation or crystal alignment (Luschen *et al.*, 1991). The orientations of such cracks are usually perpendicular to the minimum compressive stress (Batzle *et al.*, 1980; Nemat-Nasser and Horii, 1982) and the polarizations of fast/slow shear waves are observed generally parallel/perpendicular to the cracks (Crampin 1984, 1994, Crampin & Zatsepin, 1997). Occasionally this relation will be reversed in the presence of high pore-fluid pressure. The polarization of fast wave becomes perpendicular to the orientation of the cracks in what are known as 90°-flips (Zatsepin & Crampin, 1997; Angerer *et al.*, 2002; Crampin *et al.*, 2002).

At depths greater than about 500m to 1km, the minimum stress becomes horizontal. Therefore the cracks are aligned almost vertically and the rocks display an azimuth anisotropy with a vertical symmetry axis (Crampin, 1993; Crampin & Chastin, 2000). This explains why previous shear-wave analyses focus on the two horizontal components. At shallower depths, the crack orientation is more complicated and the symmetry axis may not always be vertical. In structurally complex settings the orientation of cracks may be quite variable. For some carbonates, such as oolites and coccoliths, and most shales, clays and mudstones, stress-aligned shear-wave splitting does not appear. Shales, clays and mudstones are typically composed of horizontal platelets which show strong velocity anisotropy in a vertical plane and are azimuthally isotropic (Crampin and Chastin, 2000). To address such

variations, we developed a new analysis method, based on the concept of covariance of three-component recordings, which allows the orientation and the dip of the cracks to be estimated. The stability and feasibility of this method are investigated. The preliminary results for real seismogram data are also presented

## 2. Methodology

The covariance matrix method for S-wave splitting analysis was motivated by the theory of polarization filters. This technique was first introduced into seismology by Shimshoni & Smith in 1964 to measure the rectilinearity on recorded seismograms. Various applications based on this theory were then developed to detect the phase arrivals on seismograms (*i.e.*, Lewis & Meyer, 1968; Basham & Ellis, 1969, Montalbetti & Kanasewich, 1970, Vedale, 1986). Some theoretical considerations were discussed by Samson & Olson (1980) and Kanasewich (1981). The general idea of this theory is to analyze a covariance matrix constructed from 3- (or 2-) component signals. Given a signal with three components of  $\mathbf{u}$ ,  $\mathbf{v}$ ,  $\mathbf{w}$ , its polarization can be determined by analyzing the covariance matrix  $COV$ :

$$COV = \begin{bmatrix} \langle uu \rangle & \langle uv \rangle & \langle uw \rangle \\ \langle vu \rangle & \langle vv \rangle & \langle vw \rangle \\ \langle wu \rangle & \langle wv \rangle & \langle ww \rangle \end{bmatrix} \quad (1)$$

If the polarization of signal is linear,  $COV$  just has one non-zero eigenvalue, and the corresponding eigenvector is the polarization of the signal; If the polarization of signal is planar, there are two non-zero eigenvalues, and the corresponding eigenvectors confine this plane. With these observations, the linearity  $P_l$  and planarity  $P_p$  can be defined as:

$$P_l = 1 - \frac{\lambda_2 + \lambda_3}{\lambda_1}, \quad P_p = 1 - \frac{2\lambda_3}{\lambda_1 + \lambda_2}, \quad (2)$$

where  $\lambda_1, \lambda_2, \lambda_3$  are eigenvalues of  $COV$  with  $\lambda_1 \geq \lambda_2 \geq \lambda_3$ .

Silver and Chan (1991) exploited this theory by applying it to the analysis of the shear-wave splitting in teleseismic recordings to extract the upper mantle anisotropy. But they just focused on only on the two horizontal components as previous S-splitting studies had done. Here we extend this method to process 3 components simultaneously for the cases where the symmetry axis of transverse isotropy is neither vertical nor horizontal.

The approach for applying this method to S-wave splitting analysis is to find the solutions satisfying the following condition: if the assigned time delay and slow (or fast) wave polarization are correct, then the output (or recovered) signal should be most linear- or planar-like, depending on the polarization of the incident wave.

For a linearly polarized incident wave, two steps are performed. Because the incident wave is split into fast and slow waves with orthogonal polarization directions, the particle motion of the output signal will be confined to the plane defined by those polarizations. The first step is to find the direction perpendicular to this plane. As we introduced above, this direction is the eigenvector corresponding to the minimum eigenvalue of the covariance matrix  $COV$ . We call this direction as  $V_{non}$ . After this direction is found, the signals are then projected onto the plane perpendicular to  $V_{non}$ . The second step involves rotating these two components in that plane and time-shifting one rotated component within a specified range. We then construct the covariance matrix of these two rotated and shifted components and calculate its eigenvalues. The universal minimum eigenvalue corresponds to the signals achieving the highest linearity. The corresponding eigenvector is the polarization of the incident wave, the direction on which the component was time-shifted is the polarization of the slow (or fast) wave, and the time shift is the time delay between the fast and slow waves.

For planar polarization, the splitting is determined by rotating the three components in 3D space and time-shifting each of three rotated components to achieve the highest planarity. If the time shift at one rotated component matches the time difference between fast and slow waves, and its direction is the polarization of slow wave, then one of the eigenvalues of the covariance matrix constructed from 3 component signals should be universally minimum. When a universal minimum eigenvalue is achieved, the plane defined by the two relative large eigenvalues is the particle motion plane of the incident wave.

## Program Test

The capability and stability of this method are checked for 1) noise interference, and 2) the time window size in which the signal is processed. The general scheme is to construct an artificial signal with specified polarization and time differences to test the method.

For the case of a linearly polarized incident wave, the artificial signal (Figure 1a) is constructed by projecting a linear (incident) signal onto two orthogonal directions with certain time differences. To achieve statistically meaningful results each test was simulated with 60 realizations at each noise level. The test results are given in Table 1 and Table 2. Figure 1b shows the particle motions for input and recovered signals. In Table 1 and thereafter,  $(\underline{\Omega}_{inc}, \underline{\Omega}_{inc})$  is the polarization direction of incident waves;  $(\underline{\Omega}_{slow}, \underline{\Omega}_{slow})$  is the polarization of slow wave;  $(\underline{\Omega}_{non}, \underline{\Omega}_{non})$  is the direction of  $V_{non}$ ;  $T_{diff}$  is the time difference between fast and slow waves.  $Nt1$  and  $Nt2$  in Figure 1 are the left and right boundaries of the time window in which the data are processed. The random noise level is set relative to the maximum amplitude of the input 3-component signals. The sample rate in the artificial signal is 0.01 sec. The imposed splitting model is listed in Table 1.

Table 1 shows that even with 100% noise levels (S/N=1), the estimated polarizations and time differences are very good. The errors do increase with noise, but increase very slowly. From 0% to 100% noise levels, the polarization errors are less than 10 degrees. Table 2 shows the results for different time window sizes, which is a critical free parameter in this method. We can see that as long as the window size  $(Nt2-Nt1)*dt$  is larger than  $2*T_{diff}$ , the results are always reasonable. So it can be concluded that this method should be capable of dealing with S-wave splitting and the results should be stable even for strongly interfering signals. The insensitivity of this method to noise level is extremely useful for real data processing when the S-waves are always contaminated by other phases.

We also checked the limitations of the traditional analysis method, which processes only the horizontal components. The test results are shown in Table 3. We can see that this approach can provide reasonable estimates of the polarization azimuth, but it gives poor estimates of the time difference. This method should be used with caution in a situation where the cracks are dipping.

For the case of a planar incident wave, we completed a single simulation for the noise level of 0, 5%, 20%. Figure 2 shows an example of the analysis from particle motions of input and recovered signals. Table 4 gives the results.  $(\underline{\Omega}_{nc\_norm}, \underline{\Omega}_{nc\_norm})$  is the direction perpendicular to the particle motion plane defined by the incident wave. We can say from current results that this method is feasible at least for low noise levels.

## Preliminary Results for Real Seismogram Data

We applied above method onto the seismograms recorded at a producing reservoir. There are five stations, composing a small-aperture seismic monitoring network (Figure 3). The geophones are placed in the subsurface at depths of about 150m so the recordings are free from the surface noise, and for shear-wave splitting analysis, they are also free of the distortion from the S-to-P head wave generated at the surface. A total of 12 events have been processed. The source locations are shown in Figure 3. Figure 4 shows a typical example of the seismograms and particle motions before and after shear-wave splitting analysis. After obtaining the polarization directions of the slow wave, the crack directions are determined by the rule that the polarization of the slow wave is perpendicular to the crack planes. Figure 5 shows the crack orientations and dips at each station for all 12 events. We can see the cracks have primarily NE-SW orientations and with large dipping angles for most cases. The averages of time difference per kilometer are 29.6, 71.6, 36.5, 28.5 and 54.2 ms for each of the 5 stations respectively. Due to the limited number of events, we cannot draw statistical results and temporal variations in this stage.

## Conclusions and Future Work

A new method of shear-wave splitting analysis was devised which performs on 3-component signals simultaneously. This method is capable of extracting not only the orientation, but also dipping information of cracks

in the media, superior over the traditional analysis approaches that generally process just horizontal 2 components. This method is tested very reliable and stable even for large noise.

The preliminary application to a producing reservoir shows the cracks in that area are generally NE-SW oriented with near vertical dipping. The orientation appears to be consistent with the earthquake distribution (Figure 4). Due to limited number of events, no temporal variation is resulted.

From Figure 6 we can also observe that at some stations (2, 4 and 5), the crack orientations show possible 90°-flips. As discussed by Zatsepin & Crampin (1997), and Crampin (2002). The 90°-flips may relate with the high pore-fluid pressures. The water injection at reservoir may produce high pore-fluid pressures in certain areas, and possibly caused the 90°-flips of crack directions. However, we will hold this conclusion till we get the detailed information of fluid injection in this area.

We will continue to work on this analysis program so that it will be friendly to general users. More events will be processed and the statistic analysis will be performed. The temporal variations for both crack orientation and time difference between fast and slow waves will be analyzed.

One more interested issue is to compare the results obtained here from shear-wave splitting analysis with the source mechanisms obtained from moment tensor inversion. The relative geometry between opening cracks and rupture faults is expected to reveal.

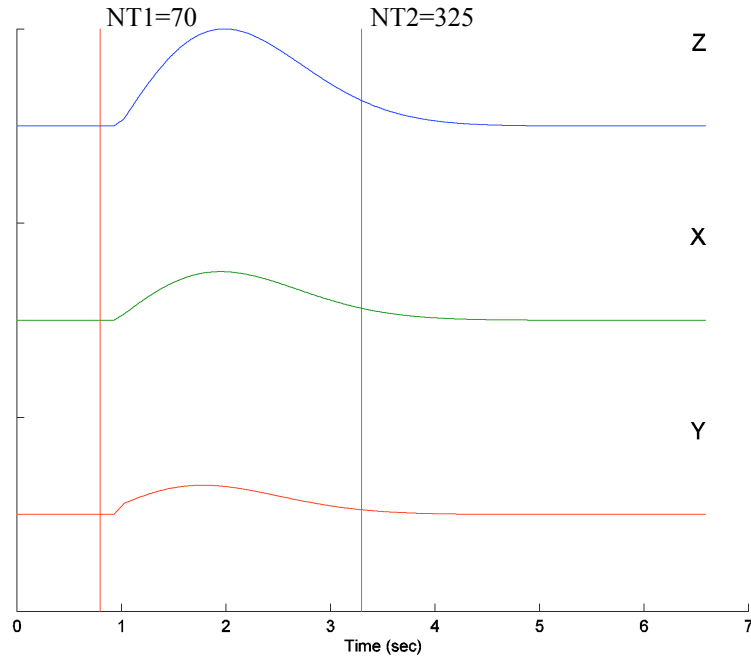
## Acknowledgements

This work was supported by the Earth Resources Laboratory Founding Member Consortium and DOE grant DE.FC03-015F22398.

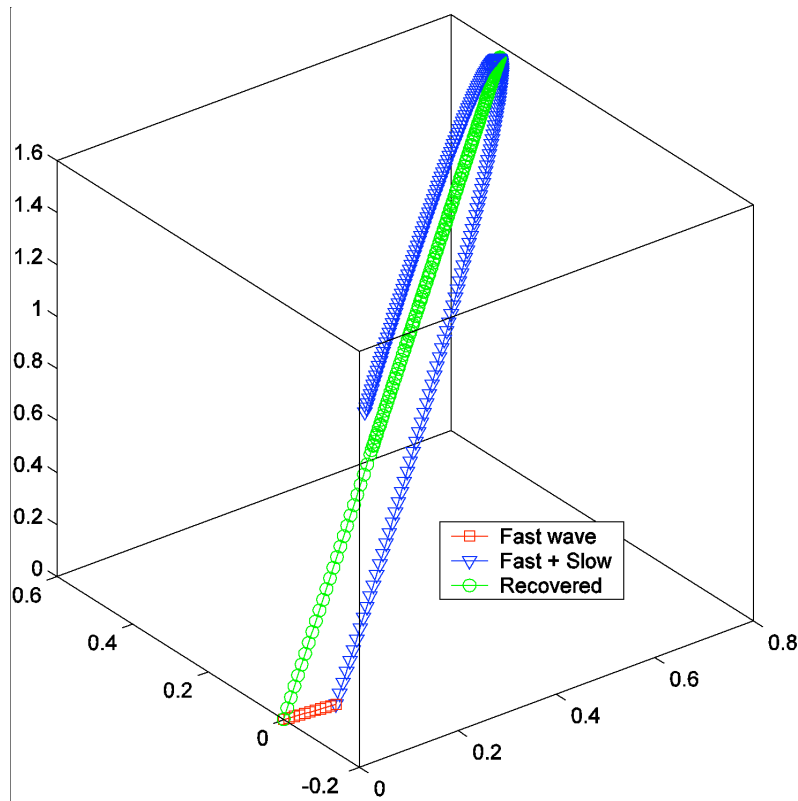
## References

- Angerer, E., S. Crampin, X.-Y. LI and T. L. Davis, 2000. Processing, modeling, and predicating time-lapse effects of over-pressured fluid-injection in a fractured reservoir. *Geophys. J. Int.*, **149**, 267-280.
- Batzle, M. L., G. Simmons and R. W. Siegfried, 1980. Microcrack closure in rocks under stress: direct observation. *J. Geophys. Res.*, **85**, 7072-7090.
- Crampin, S. and J. H. Lovell, 1991. A decade of shear-wave splitting in the Earth's crust: what does it mean? what use can we make of it? and what should we do next?. *Geophys. J. Int.*, **107**, 387-407.
- Crampin, S. and S. V. Zatsepin, 1997. Modelling the compliance of crustal rock, II-response to temporal changes before earthquakes. *Geophys. J. Int.*, **129**, 495-506.
- Crampin, S. T. Volti and R. Stefansson, 1999. A successfully stress-forecast earthquake. *Geophys. J. Int.*, **138**, F1-F5.
- Crampin, S., 1984. Evaluation of anisotropy by shear-wave splitting. *Geophysics*, **50**, 142-152.
- Crampin, S., 1993. Arguments for EDA. *Can. J. expl. Drill.*, **1**, 21-26.
- Crampin, S., 1994. The fracture criticality of crustal rocks. *Geophys. J. Int.*, **118**, 428-438.
- Crampin, S., R. Evans and B. K. Atkinson, 1984. Earthquake predication: a new physical basis. *Geophys. J. R. astr. Soc.*, **76**, 147-156.
- Crampin, S., T. Volti, S. Chastien, A. Gudmundsson and R. Stefansson, 2002. Indication of high pore-fluid pressure in a seismically-active fault zone. *Geophys. J. Int.*, **151**, F1-F5.
- Crampin, S., 1993. Arguments for EDA. *Can. J. expl. Drill.*, **1**, 21-26.
- Crampin S. and S. Chastin, 2000. Shear-wave splitting in a critical crust: II-compliant, calculable, controllable, fluid-rock interactions. in *Anisotropy 2000: Fractures, converted waves and case studies*, published by *The Society of Exploration Geophysicists*. pp 21-28.
- Gao, Y., P. Wang, S. Zheng, M. Wang, Y. Chen and H. Zhou, 1998. Temporal changes in shear-wave splitting at an isolated swarm of small earthquakes in 1992 near Dongfang, Hainan Island, southern China. *Geophys. J. Int.*, **135**, 102-112.
- Kanasewich, E. R., 1981. *Time Sequence Analysis in Geophysics*, University of Alberta Press, Edmonton, Canada.
- Kaneshima, S., 1990. Origin of crustal anisotropy: shear wave splitting studies in Japan. *J. Geophys. Res.*, **95**, 11,121-11,133.

- Luschen, E, W. Sollner, A. Hohrath and W. Rabbel, 1991. Integrated P- and S-wave borehole experiments at the KTB-Deep Drilling Site in the Oberpfalz area (SE Germany), in *Continental Lithosphere: Deep Seismic Reflections, Geodynamics*, **22**, 121-133.
- Menke, William and Vadim Levin, 2003. The cross-convolution method for interpreting SKS splitting observations, with application to one and two-layer anisotropic earth models. *Geophys. J. Int.*, **154**, 379-392.
- Montalbetti, J. R. and E. R. Kanasewich, 1970. Enhancement of teleseismic body phases with a polarization filter. *Geophys. J. R. astr. Soc.*, **21**, 119-129.
- Nemat-Nasser, S., and H. Horii, 1982. Compression-induced non planar crack extension with application to splitting, exfoliation, and rockburst. *J. Geophys. Res.*, **87**, 6805-6821.
- Rengin Gok, J. F. Ni, M. West, E. Sandvol, D. Wilson, R. Aster, W. S. Baldrige, S. Grand, W. Gao, F. Tillmann and S. Semken, 2003. Shear wave splitting and mantle flow beneath LA RISTRA. *Geophys. Res. Lett.*, **30**, 1-4.
- Samson, J. C. and J. V. Olson, 1980. Some comments on the description of polarization states of waves. *Geophys. J. R. astr. Soc.*, **61**, 115-129.
- Shimshoni, M. & S. W. Smith, 1964. Seismic signal enhancement with three component detectors. *Geophysics*, **29**, 664-671.
- Silver, P. and W. W. Chan, 1991. Shear wave splitting and subcontinental mantle deformation. *J. Geophys. Res.*, **96**, 16429-16454.
- Vedale, J. E., 1986. Complex polarization analysis of particle motion. *Bull. Seism. Soc. Am.*, **76**, 1393-1405.
- Zatsepin, S. V. and S. Crampin, 1997. Modeling the compliance of crustal rock: I- response of shear-wave splitting to differential stress. *Geophys. J. Int.*, **129**, 477-494.

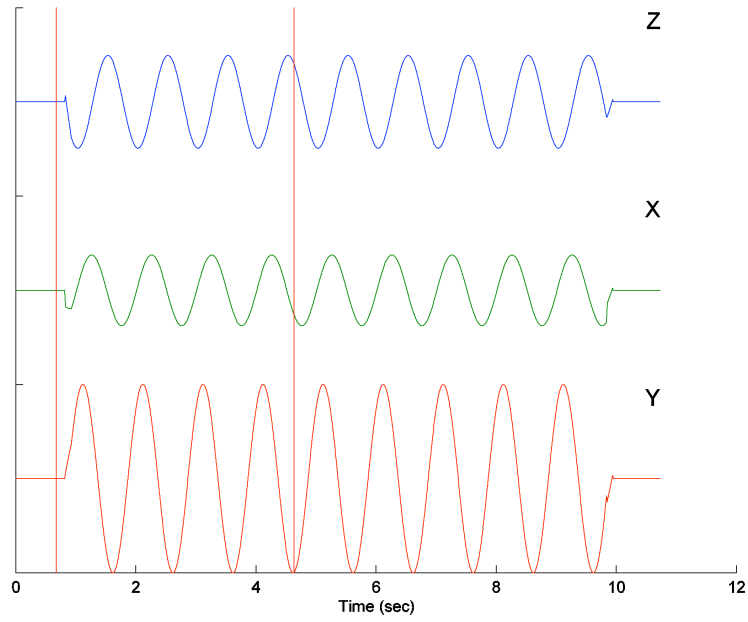


(a)

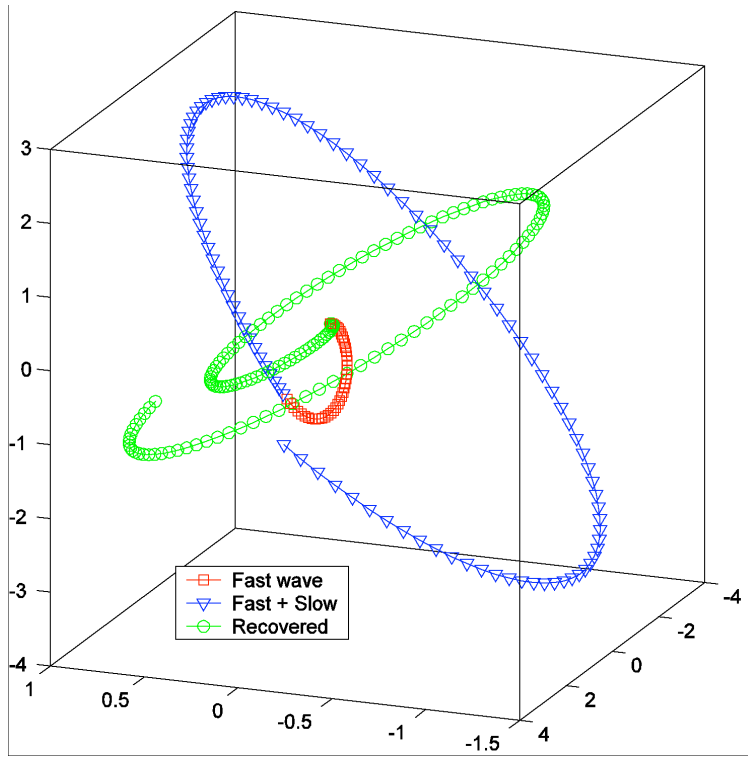


(b)

**Figure 1.** The case of linear polarized incident wave. (a) The artificial 3-component signal with splitting parameters given in table 1. (b) Particle motions of artificial signal and recovered signal. After right time was shifted back along slow wave direction, the recovered particle motion is perfect linear (green curve).



(a)



(b)

**Figure 2.** The case for planar polarized incident wave. (a) The 3-component of artificial input signal. (b) Particle motions of artificial signal and recovered signal. After right time was shifted back along slow wave direction, the recovered particle motion is perfectly confined in one plane (green curve).

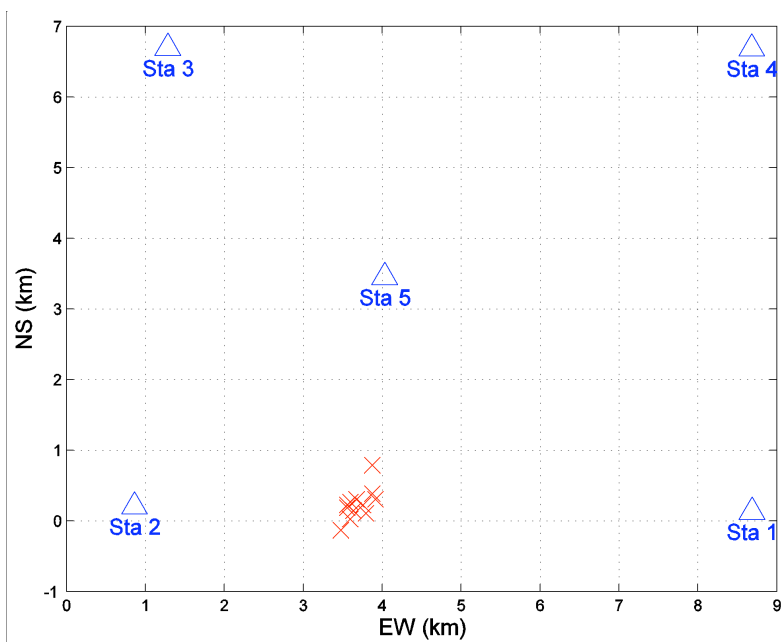


**Figure 3.** The locations of 5 stations (blue triangles) and 12 processed events (red crosses).



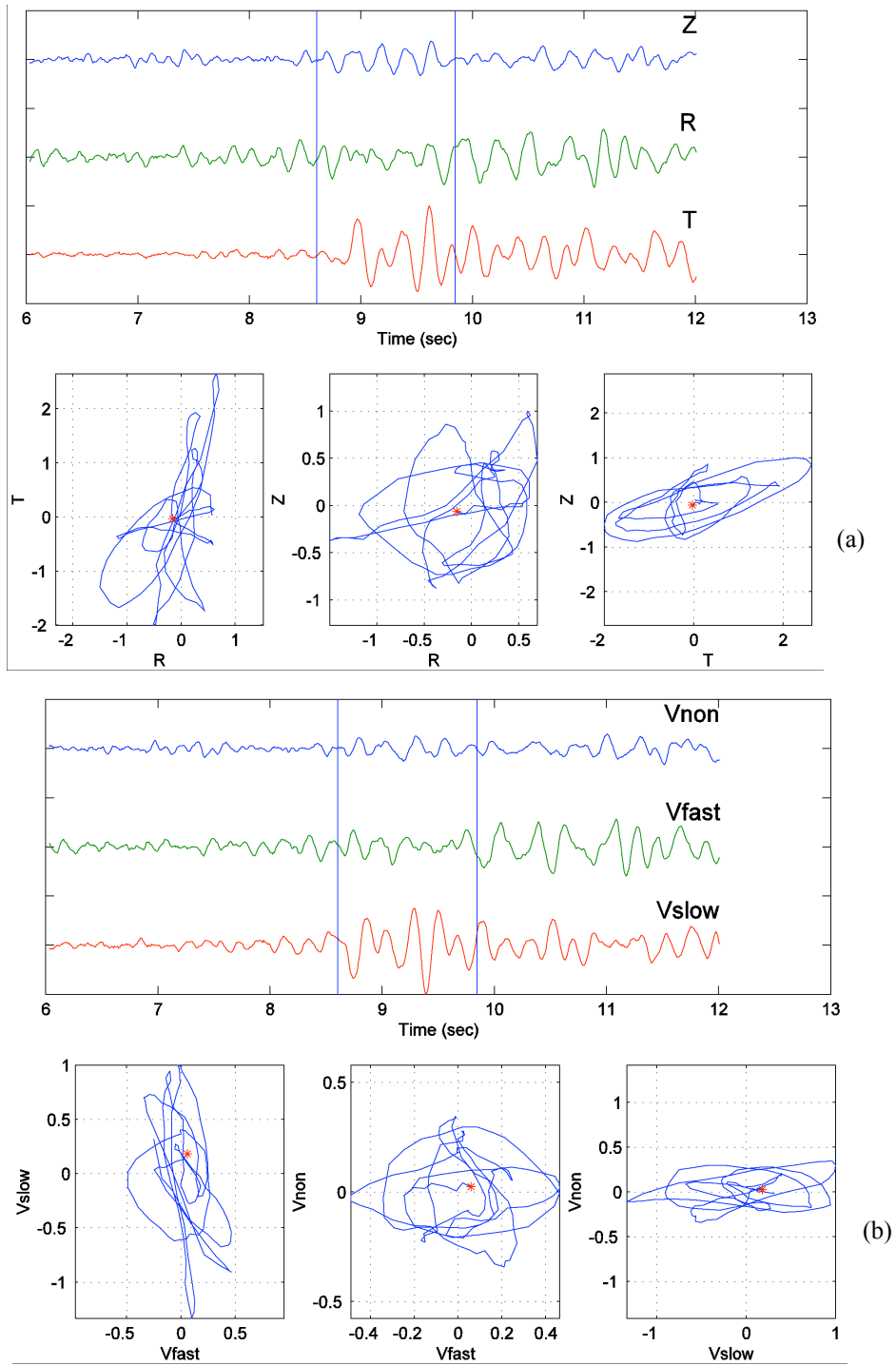


**Figure 4.** One example of seismograms and particle motions before (a) and after (b) shear-wave splitting analysis for station 4.

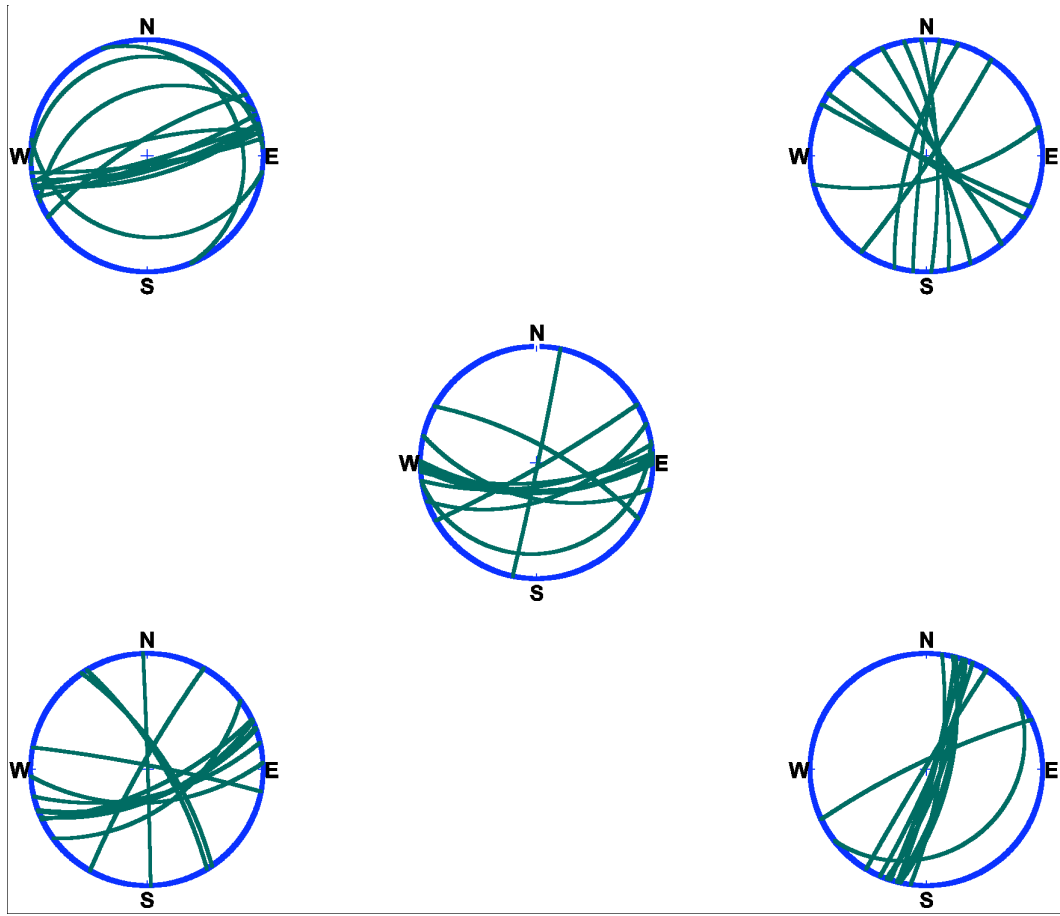


**Figure 5.** Lower hemisphere equal-area pole projection of cracks at location of each station for all 12 events resulted from shear-wave splitting analysis.

**Table 1.** Test results for different noise levels for fixed time window (Nt1=70, Nt2=300)

Model	30	30	60	60	68.54	343.19	0.40		
Noise	$\underline{\mu}_{inc}(^{\circ})$	$\underline{\mu}_{inc}(^{\circ})$	$\underline{\mu}_{slow}(^{\circ})$	$\underline{\mu}_{slow}(^{\circ})$	$\underline{\mu}_{non}(^{\circ})$	$\underline{\mu}_{non}(^{\circ})$	$T_{diff}(sec)$	$P_l$	$P_p$
0%	29.98+-0.00	29.95+-0.00	59.75+-0.00	59.86+-0.00	68.44+-0.00	343.19+-0.00	0.40+-0.00	1.000+-0.000	1.000+-0.000
10%	30.06+-0.16	30.02+-0.34	60.36+-1.16	60.09+-0.69	68.44+-0.25	343.09+-0.61	0.40+-0.01	0.999+-0.000	0.999+-0.000
20%	29.99+-0.35	29.93+-0.64	59.86+-2.35	59.57+-1.35	68.59+-0.46	342.77+-1.21	0.40+-0.02	0.995+-0.000	0.996+-0.000
30%	30.03+-0.43	30.00+-1.07	60.12+-3.60	59.84+-2.28	68.49+-0.78	343.04+-1.83	0.40+-0.03	0.990+-0.001	0.991+-0.000
40%	30.02+-0.66	30.36+-1.52	61.29+-4.71	60.39+-3.59	68.72+-1.12	342.82+-2.67	0.40+-0.04	0.982+-0.001	0.985+-0.001
50%	29.97+-0.81	30.10+-1.82	61.14+-6.20	60.37+-3.83	68.60+-1.46	343.10+-3.57	0.41+-0.05	0.972+-0.002	0.977+-0.001
60%	30.44+-1.01	30.50+-2.49	63.42+-8.44	60.40+-5.74	68.92+-2.02	341.79+-4.82	0.42+-0.07	0.961+-0.002	0.967+-0.002
70%	30.30+-1.14	30.02+-2.32	63.65+-8.73	61.71+-6.72	68.30+-2.54	343.38+-6.46	0.42+-0.07	0.947+-0.004	0.956+-0.003
80%	30.19+-1.47	30.42+-2.70	65.44+-9.88	60.98+-7.00	69.44+-2.88	343.20+-7.78	0.41+-0.08	0.932+-0.004	0.943+-0.004
90%	30.14+-1.71	30.64+-3.24	63.50+-10.79	62.49+-8.19	68.49+-3.26	343.16+-11.20	0.43+-0.11	0.914+-0.006	0.931+-0.005
100%	30.08+-1.61	30.68+-3.30	64.70+-10.30	62.16+-8.78	69.15+-3.92	342.32+-10.15	0.40+-0.09	0.899+-0.008	0.915+-0.007

**Table 2.** Test results for different time windows (NT1=70) with fixed noise level of 50%.

NT2	$\underline{\mu}_{inc}(^{\circ})$	$\underline{\mu}_{inc}(^{\circ})$	$\underline{\mu}_{slow}(^{\circ})$	$\underline{\mu}_{slow}(^{\circ})$	$\underline{\mu}_{non}(^{\circ})$	$\underline{\mu}_{non}(^{\circ})$	$T_{diff}(sec)$	$P_l$	$P_p$
150	35.24+-19.90	38.51+-23.72	72.62+-19.34	67.79+-16.55	69.80+-4.66	341.71+-24.41	0.50+-0.16	0.936+-0.021	0.954+-0.014
175	32.33+-4.73	34.70+-7.07	71.55+-17.01	66.06+-8.94	68.65+-1.49	344.30+-8.17	0.50+-0.14	0.962+-0.010	0.971+-0.008
200	31.11+-2.44	31.27+-4.16	66.41+-9.96	62.36+-6.85	68.54+-1.50	342.56+-6.64	0.42+-0.09	0.972+-0.004	0.978+-0.003
225	30.37+-1.34	30.32+-2.40	63.49+-7.48	61.04+-4.83	68.59+-1.44	342.62+-4.76	0.40+-0.05	0.976+-0.002	0.980+-0.002
250	30.40+-1.42	30.38+-2.49	64.89+-10.85	61.44+-5.80	68.70+-1.77	342.40+-4.79	0.41+-0.08	0.975+-0.003	0.980+-0.002
275	30.07+-0.99	30.00+-1.63	61.05+-7.02	60.31+-4.51	68.45+-1.68	343.25+-4.54	0.41+-0.05	0.974+-0.002	0.978+-0.001
300	30.22+-0.88	30.21+-1.84	61.86+-6.00	61.13+-4.39	68.24+-1.56	343.69+-4.39	0.41+-0.04	0.972+-0.002	0.977+-0.001
325	30.12+-1.01	29.97+-1.94	62.72+-8.21	60.94+-5.30	68.48+-1.45	342.90+-3.11	0.41+-0.07	0.970+-0.002	0.975+-0.002
350	30.04+-0.90	30.23+-1.83	62.53+-6.63	61.60+-3.54	68.34+-1.53	343.78+-3.27	0.40+-0.05	0.967+-0.002	0.972+-0.001
375	30.02+-0.81	30.07+-1.64	59.49+-5.18	60.23+-3.72	68.20+-1.41	344.05+-3.50	0.42+-0.05	0.964+-0.002	0.969+-0.002
400	30.07+-0.89	30.37+-1.91	62.31+-7.77	61.41+-4.54	68.41+-1.68	343.74+-4.12	0.41+-0.06	0.961+-0.002	0.967+-0.002

**Table 3.** Test results for traditional 2-component analysis method with noise level of 20% and window size of (nt1=70, Nt2=300).

<i>Noise</i>	$\bar{\Pi}_{nc}(^{\circ})$	$\bar{\Pi}_{slow}(^{\circ})$	$T_{diff}(sec)$
0%	31.32+-0.00	57.00+-0.00	0.60+-0.00
10%	31.40+-0.65	57.00+-1.22	0.61+-0.02
20%	31.61+-1.21	57.52+-2.50	0.60+-0.04
30%	31.78+-2.35	58.18+-4.59	0.60+-0.05
40%	31.72+-3.22	58.62+-5.78	0.60+-0.06
50%	33.23+-3.82	62.10+-8.00	0.58+-0.07
60%	34.21+-5.93	67.98+-16.12	0.56+-0.09
70%	35.47+-6.81	69.68+-17.10	0.60+-0.07
80%	36.38+-6.75	73.60+-16.01	0.53+-0.11
90%	33.85+-8.23	68.93+-18.26	0.54+-0.10
100%	34.49+-8.92	71.20+-19.22	0.55+-0.12

**Table 4.** Test results for planar polarization of incident wave with different noise levels.

<b>Parameter</b>	<b>Model</b>	<b>Noise=0%</b>	<b>Noise=5%</b>	<b>Noise=20%</b>
$\bar{\Pi}_{nc \text{ norm}}(^{\circ})$	30	30	32.55	24.51
$\bar{\Pi}_{nc \text{ noerm}}(^{\circ})$	30	30	35.04	42.70
$\bar{\Pi}_{slow}(^{\circ})$	60	60	59	55
$\bar{\Pi}_{slow}(^{\circ})$	60	60	68	72
$T_{diff}(sec)$	0.4	0.4	0.41	0.42